Control of carbon nanostructure: From nanofiber toward nanotube and back

A. V. Melechko[a)]
Material Science and Technology Division, and Center for Nanophase Materials Sciences, Oak Ridge National Laboratory, Oak Ridge, Tennessee 37831, USA

K. L. Klein and J. D. Fowlkes
Department of Materials Science and Engineering, University of Tennessee, Knoxville, Tennessee 37996-2200, USA and Center for Nanophase Materials Sciences, Oak Ridge National Laboratory, Oak Ridge, Tennessee 37831, USA

D. K. Hensley
Center for Nanophase Materials Sciences, Oak Ridge National Laboratory, Oak Ridge, Tennessee 37831, USA

I. A. Merkulov[b)]
Ioffe Physico-Technical Institute, Russian Academy of Sciences, St.-Petersburg, Russia

T. E. McKnight
Engineering Science and Technology Division, Oak Ridge National Laboratory, Oak Ridge, Tennessee 37831, USA

P. D. Rack
Department of Materials Science and Engineering, University of Tennessee, Knoxville, Tennessee 37996-2200, USA and Center for Nanophase Materials Sciences, Oak Ridge National Laboratory, Oak Ridge, Tennessee 37831, USA

J. A. Horton
Material Science and Technology Division, Oak Ridge National Laboratory, Oak Ridge, Tennessee 37831, USA

M. L. Simpson
Material Science and Technology Division, and Center for Nanophase Materials Sciences, Oak Ridge National Laboratory, Oak Ridge, Tennessee 37831, USA, and Department of Materials Science and Engineering, University of Tennessee, Knoxville, Tennessee 37996-2200, USA

(Received 2 March 2007; accepted 6 August 2007; published online 12 October 2007)

The unique properties of carbon nanofibers (CNFs) make them attractive for numerous applications ranging from field emitters to biological probes. In particular, it is the deterministic synthesis of CNFs, which requires precise control over geometrical characteristics such as location, length, diameter, and alignment, that enables the diverse applications. Catalytic plasma enhanced chemical vapor deposition of vertically aligned CNFs is a growth method that offers substantial control over the nanofiber geometry. However, deterministic synthesis also implies control over the nanofiber's physical and chemical properties that are defined by internal structure. Until now, true deterministic synthesis has remained elusive due to the lack of control over internal graphitic structure. Here we demonstrate that the internal structure of CNFs can be influenced by catalyst preparation and ultimately defined by growth conditions. We have found that when the growth rate is increased by 100-fold, obtained through maximized pressure, plasma power, and temperature, the resulting nanofibers have an internal structure approaching that of multiwalled nanotubes. We further show that the deliberate modulation of growth parameters results in modulation of CNF internal structure, and this property has been used to control the CNF surface along its length for site specific chemistry and electrochemistry. © *2007 American Institute of Physics*. [DOI: 10.1063/1.2786710]

I. INTRODUCTION

Although many nanomaterials research efforts largely focus on the synthesis and characterization of new nanomaterials, the highest levels of functionality are envisioned from the collective behaviors of interacting nanoscale components where scale and complexity lead to "entirely new properties."[1] The challenge then is not just one of the synthesis of nanomaterials, but also one of how these materials should be organized into ensembles that exhibit new levels of functionality. Addressing this question shifts the focus to the controlled synthesis and directed assembly of systems of nanoscale components that are capable of assuming a high level of organization. By controlled synthesis we mean a process of collective nanostructure growth where the perti-

[a)]Electronic mail: acm@ornl.gov
[b)]Consulting for Materials Science and Technology Division, Oak Ridge National Laboratory, Oak Ridge, Tennessee 37831.

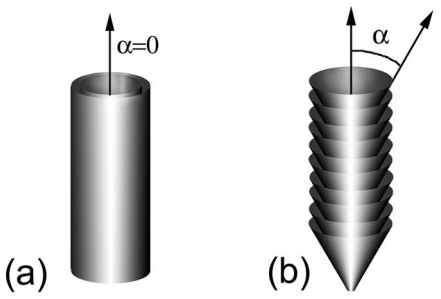

FIG. 1. Schematic definition of a (a) carbon nanotube and (b) carbon nanofiber.

nent attributes (location, size, orientation, composition, electrical, mechanical, and thermal properties, etc.) of the individual elements can be selected *a priori* by the choice of the growth conditions or the preparation of the growth substrate. The controlled synthesis of carbon nanostructures, in particular, has its own set of challenges.

The bonding properties of carbon endow it with the ability to form a large variety of crystal structures.[2] Discovery of its sp^2-bonded closed forms (fullerenes) that include buckyballs[3] and nanotubes[4] has attracted interest due to their mechanical strength and chemical stability. These structures, however, do not exhaust all possible configurations that can be derived from a graphene sheet.[5] Graphene is a planar hexagonal network of carbon atoms terminated by hydrogen atoms. A carbon nanotube can be considered as a graphene sheet rolled into a cylinder [Fig. 1(a)], while introduction of five and seven member rings into graphene allows the formation of curved structures such as buckyballs[3] and nanocones.[6] Carbon nanofibers (CNFs) are a class of materials that have curved graphene layers stacked to form a quasi-one-dimensional "filament," and the internal nanofiber structure can be characterized by the angle α between the graphene layers and the fiber axis [Fig. 1(b)]. In the case of true carbon nanotubes, α is zero. Despite distinct differences in their internal structures, nanofibers are often called nanotubes as they can display similar morphology. However, the physical and chemical properties of nanofibers are quite different from nanotubes. While nanotubes are reported to display ballistic electron transport[7] and diamondlike tensile strength along the axis,[8] nanofibers have proven their robustness as individual, free-standing structures with higher chemical reactivity and electron transport across their sidewalls, important for functionalization[9–12] and electrochemical applications,[13–15] respectively.

Many different variations in the internal structure of CNFs have been observed throughout the literature.[16,17] Here we refer to two commonly identified configurations: herringbone-type, in which dense, conical graphene layers resemble a fish skeleton when viewed in transmission, and bamboo-type (more similar to a nanotube), in which cylindrical, cuplike graphene layers alternate with cavities along the length, thus resembling the cross section of a bamboo stem. Variation of the internal graphitic structure of the nanofiber inevitably results in a variation of the surface structure. True nanotubes have graphitic basal planes exposed with very few chemically active defect sites, whereas nanofiber surfaces consist mainly of hydrogen terminated graphitic edges, which are more amenable to chemical modification. Furthermore, even though both herringbone and bamboo structures contain many defects, the herringbone type has more graphitic planes ending on the outer walls of the fiber and is therefore thought to contain more active sites at the surface. Maximizing the number of attachment sites and minimizing contamination of the surface have proven to be big obstacles for chemically functionalizing surfaces for biological applications. Similarly, graphitic structure also affects electron transport along the length of the fiber and at the surface. Since electron transfer rates on edge planes are typically orders of magnitude faster than at basal planes,[18] one would expect much higher electron transport in regions featuring high densities of graphitic edge planes (i.e., herringbone structure).

Over the past few years it has been demonstrated that vertically aligned CNFs (VACNFs) can be synthesized almost deterministically by catalytic plasma enhanced chemical vapor deposition (C-PECVD).[19,20] In this synthesis process, the precise location of the VACNF can be defined by patterning the catalyst thin film using photolithography or electron beam lithography, while the diameter and density of nanofibers arranged in a stochastic array or "forest" is controlled by the thickness of the unpatterned catalyst film.[21] Nanofiber height is specified by the growth rate and duration of the growth process and the vertical alignment of the fibers is maintained by the electric field present in the plasma sheath. Due to this considerable level of control during the synthesis process, the technology of VACNF synthesis has matured to the point that it can be used as a standard processing step in complex device fabrication.[15,22–27] Yet true controlled synthesis has not been demonstrated as command of the internal graphitic structure of the nanofibers, which controls mechanical strength, electron transport, and surface chemistry, has remained elusive. In catalytic thermal CVD processes, the structure and properties of the fibers can be influenced by a number of factors, including the nature of the metal surface, the composition of the gas-phase reactant, the temperature, and the incorporation of either gas phase or solid additive.[17] However, other important properties such as alignment are not controllable in thermal CVD. Here we demonstrate that the internal structure of vertically aligned CNFs can be controlled by the preparation of catalyst nanoparticles with defined crystallographic structure and orientation, and by the selection of growth conditions. We have found that the selection of growth conditions corresponding to the highest growth rate results in nanofibers with an internal structure approaching that of nanotubes. Even though crystallographic and morphological properties of the catalyst nanoparticle definitively influence the internal structure of the CNF, ultimately the growth conditions are the overriding factor.

II. RESULTS AND DISCUSSION

VACNFs were synthesized from Ni and Fe thin films evaporated directly onto *n*-type Si (100) substrates. No pretreatment of the silicon substrate was performed prior to

metal deposition, leaving the native silicon oxide layer intact. In the PECVD chamber, the sample was heated to 700 °C and pretreated in an ammonia (80 sccm flow rate) plasma at 3 Torr, 200 mA for 1 min to facilitate the formation of catalyst particles from the continuous metal film. Next, acetylene was introduced to the plasma at 40 sccm, initiating the growth of nanofibers. Following a 10 min growth, the sample was imaged using scanning electron microscopy (SEM, Hitachi S4700), scanning transmission electron microscopy (STEM, Hitachi HD-2000), and high-resolution transmission electron microscopy (HRTEM, Hitachi HF-2000). For cross sectional SEM, the silicon substrate was cleaved in the middle for imaging in the direction perpendicular to nanofibers. For STEM and TEM analysis, the nanofibers were removed from the substrate and transferred to lacey carbon-coated TEM grids.

Nanofibers grown from 10 nm Ni films, shown in Fig. 2(a), display a noticeable variation in height. Careful inspection of Fig. 2(a) shows that the majority of nanofibers on average have one height with a portion of the population having grown taller, suggesting a bimodal distribution. This visual observation is supported by a histogram of the height distribution as presented in Fig. 2(b). Curve fitting with two Gaussian functions (green and blue curves) gives 0.8 and 1 μm height centers for each distribution component. Heights were measured only on the nanofibers that are in the line of view and in focus, thus some of the shorter fibers may not be accounted for in the statistical distribution. Top-view SEM inspection [Fig. 2(c)] of the nanoparticle at the tips of the fibers reveals that some of the nanoparticles form a complete or a partial hexagon geometry, while other nanoparticles have a square shape. This faceting suggests that the nanoparticles are oriented with respect to the substrate, with the hexagonally shaped particles indicating that the ⟨111⟩ direction is perpendicular to the surface and the square shaped particles indicating a ⟨100⟩ orientation for fcc Ni. Some particles have an unidentifiable shape that is not suggestive of crystallographic orientation. Examination of the nanoparticles by STEM revealed the difference in the transverse geometry of the nanoparticles. Two varieties of nanoparticle shapes were identified [Fig. 2(d)]: (1) conical with sloping sides interfacing to the fiber; and (2) rectangular shaped with sides almost parallel to the axis of the fiber. This difference in nanoparticle geometry is reflected in the structure of the graphene layers, with the conical particles producing a herringbonelike fiber structure and rectangular particles producing a bamboolike fiber structure. This result illustrates that the crystallographic orientation of the nanoparticle plays a critical role in the resultant CNF structure. Our previous work demonstrated that the orientation texture of the nanoparticles can be preserved throughout the nanofiber growth process.[28] Preparation of catalyst films with preferred crystallographic orientation would enable the synthesis of VACNFs with a uniform internal structure. Physical vapor depositions methods allow for a degree of orientation texture control. The prevalent orientation of the catalyst film depends on the thin film deposition conditions, such as pressure, temperature, and bias. X-ray diffraction studies confirmed the prevalence of ⟨111⟩ and ⟨200⟩ in the mixture of

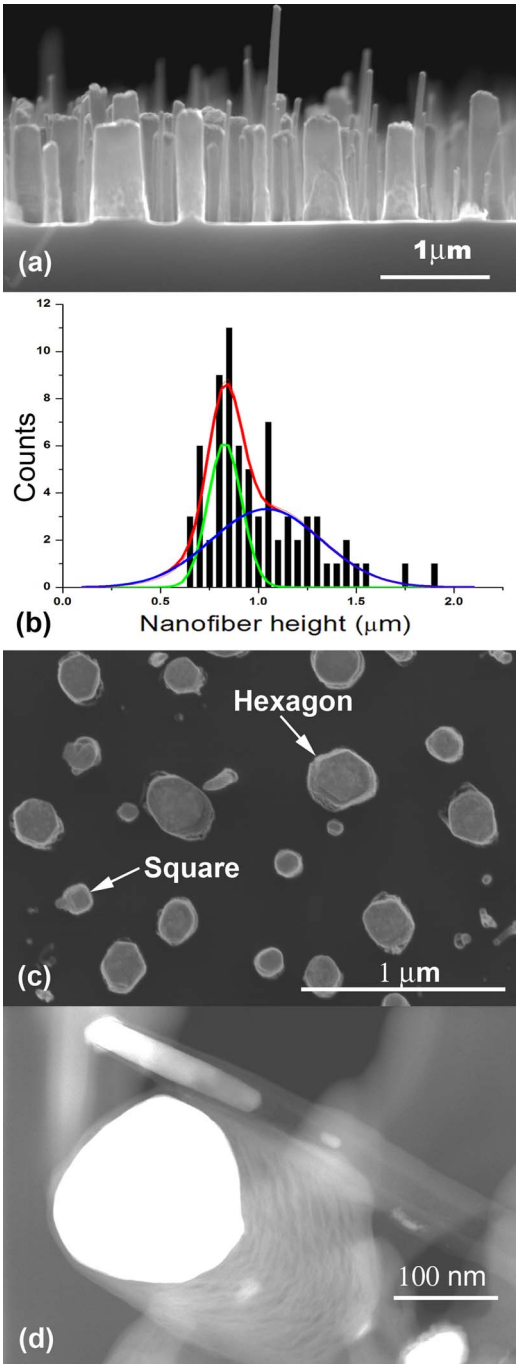

FIG. 2. (Color online) Two possible types of VACNFs synthesized from a 10 nm Ni thin film on Si(100): (a) SEM cross sectional image showing difference in fiber heights; (b) histogram of nanofiber height distribution: total curve (red) can be split into bimodal components (green and blue curves) with centers at 0.8 and 1 μm tall; (c) SEM top view image of nanofiber tips with equilibrium-shaped particles; (d) STEM image of nanofibers with two types of particle geometries and their corresponding nanofiber internal structures (herringbone and bamboo).

orientation textures in Ni films deposited by magnetron sputtering.[28] In contrast, the nanofibers grown from electroplated films were reported to exhibit a large variation of nanoparticle orientations.[29]

Elemental composition and crystallographic phase also influence the catalyst nanoparticle shape. The metals that catalyze CNF growth include several elemental transition metals, including Ni, Fe, Co, Pt, Pd, Ru, their alloys, and

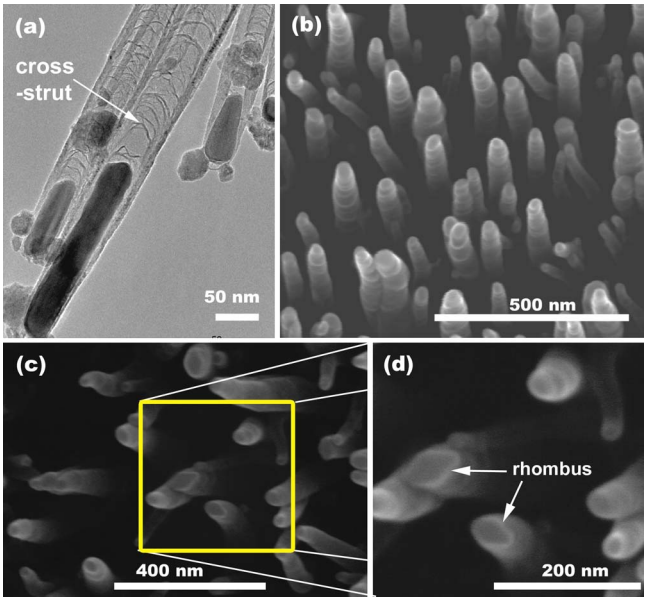

FIG. 3. (Color online) Structure and morphology of Fe catalyst nanoparticles: (a) TEM image of Fe nanoparticles at the tips of bamboo CNFs (cross strut indicated by an arrow); (b) SEM image at a 30° view of Fe-catalyzed CNFs showing the corrugated bamboolike appearance of the nanofiber sidewalls; (c) top view of Fe nanoparticles; and (d) higher magnification of the boxed area indicated in (c), exhibiting rhombus-shaped particles.

alloys with metals that alone are not catalytic, such as Cr and Cu.[30–34] Here we provide a qualitative comparison between Ni and Fe catalysts. Figure 3 shows nanofibers that were grown from a 5 nm Fe film deposited on a Si (100) substrate with the same fiber growth conditions as given above. The Fe catalyst invariably produces bamboolike nanofibers, while both bamboo and herringbone nanofibers may be grown from Ni catalyst. The internal structure of Fe-catalyzed nanofibers consist of sections of graphene cups with a very small cone angle, and are thus more cylindrical (or nanotubelike) than conical [Fig. 3(a)]. The bottoms of these graphitic cups consist of curved sections across the center of the nanofiber, which we refer to as cross struts. The SEM image in Fig. 3(b) is taken at 30° viewing angle to show the corrugated bamboolike appearance of the nanofiber sidewalls. A top view of the Fe nanoparticles is shown in Fig. 3(c) and the inset of Fig. 3(d), which reveals that they have a preferred faceting geometry of a rhombus with rounded vertices. The absence of observed herringbone-type fibers is consistent with the observation that Fe more readily catalyzes the formation of nanotubes than Ni, which is reflected in Fe being the most common catalyst for the production of carbon nanotubes. Even in thermal CVD processes it has been shown that in some cases Ni forms herringbone structures instead of nanotubes, while Fe and Co produce nanotubes at the same conditions.[35]

However, regardless of the initial catalyst preparation, growth conditions have an overriding influence on nanofiber structure. The formation of graphite layer-by-layer occurs in an asymmetrical fashion as there is a significant difference between in-plane (tangential, v_t) and out-off-plane (normal, v_n) growth velocities [Fig. 4(a)]. Helveg *et al.*[36] observed that carbon incorporation into a growing nanofiber is faster

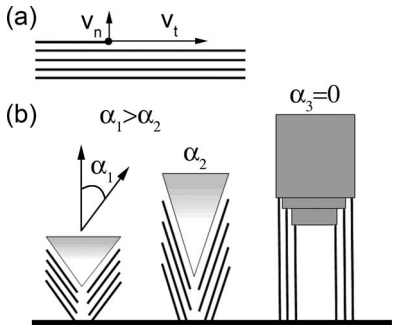

FIG. 4. (a) Diagram indicating the difference of the growth rates ($v_t \gg v_n$) in the layer-by-layer growth of graphite, where v_t is the tangential velocity and v_n is the normal velocity; (b) schematic of the nanofiber growth rate dependence on the cone angle α.

along the graphene plane (parallel to the catalyst surface) than in the perpendicular direction, and inspection of Fig. 2(d) shows that the taller nanofiber has graphene layers with a smaller cone angle with respect to the nanofiber axis than does the shorter nanofiber. Based on this observation, it appears likely that the growth rate of CNFs depends on the angle between the graphene layers and axis of a nanofiber [Fig. 4(b)], and we hypothesized that the inverse (graphitic structure of the fiber depends on the growth rate) also holds true. Calculations based on a phenomenological model of the evolution of growth interface with curvature dependent velocity v_n (Ref. 39) predict that drastic changes in the shape of the interface can occur under certain conditions. Although this model shows a complex relationship between nanofiber growth rate and internal structure, the specific relationship may not be imperative, as one might expect in general that growth conditions corresponding to a higher growth rate will produce nanofibers having an internal structure with a smaller cone angle α.

We and others have shown experimentally that the growth rate can be varied with PECVD synthesis parameters such as temperature, total pressure, total gas flow rate, gas flow ratio, and plasma power.[21,37,38] The dependence on temperature has a maximum around 700 °C,[21,40] as the carbon diffusion rate increases with temperature, while the sticking coefficient of carbon species to the catalyst surface decreases with increasing temperature. An increase in the total gas flow rate also raises the growth rate,[41] as this results in a faster supply rate of carbon source material to the catalyst surface. Most importantly, though, Chhowalla *et al.* showed that the nanofiber growth rate increases almost linearly with pressure up to at least 10 Torr.[21] The growth rate continues to increase at higher pressures. However, optimization of growth is complicated as these parameters are interlinked and maximization has to be performed in a multidimensional space.[21,41,42]

We performed a growth rate maximization procedure based on the known empirical trends in growth conditions described above. The starting point for the growth parameters was 3 Torr total pressure, 40 sccm C_2H_2, 80 sccm NH_3, 400 mA current, and 700 °C. This recipe results in standard herringbone-type nanofibers grown from a 50 nm Ni catalyst film, as shown in Figs. 5(a) and 5(b). After each growth attempt lasting 10 min, the nanofibers were inspected in the

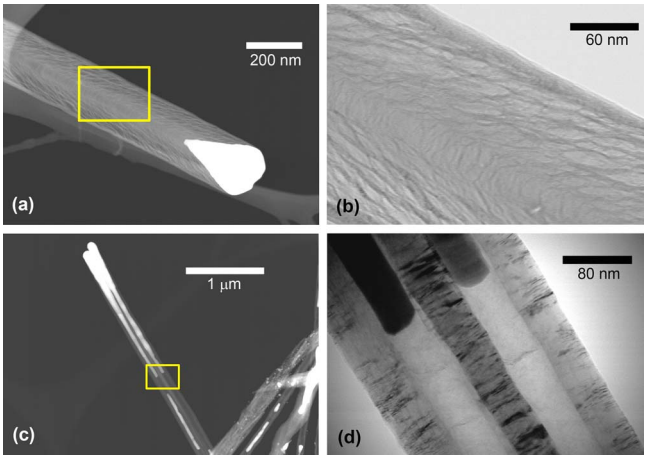

FIG. 5. (Color online) STEM analysis of Ni-catalyzed CNF internal structure: (a) *z*-contrast image of a nanofiber and a catalytic particle grown by the slow regime displaying a herringbone structure with a large cone angle; (b) transmission image at higher magnification of (a); (c) *z*-contrast image of two nanofibers grown in fast regime, displaying a bamboo-type, almost nanotubelike, structure with a small cone angle; (d) transmission image at higher magnification of (c).

SEM and the growth rate was determined based on the measurement of the average nanofiber height. The growth rate maximization strategy involved stepwise changes in total gas flow rate, substrate temperature, total pressure, and plasma current. At every new set of parameters the growth rate was maximized by varying the NH_3/C_2H_2 gas flow ratio. Since it has been shown that the growth rate increases with gas flow rate, the total gas flow rate was increased to the limit of the mass flow controllers ~300 sccm (a true maximum flow rate was not achievable in this study due to limitations of the available mass flow controllers and the showerhead configuration). The growth rate increased monotonically with pressure, however, all of the other parameters had to be optimized at each new pressure setting; the increase in pressure had to be accompanied with an increase in plasma power to maintain the glow discharge, and since plasma power inevitably influenced the actual substrate temperature, the search in heater temperature was repeated. Part of this maximization procedure was performed in one reactor that was equipped to work with pressures below 10 Torr and power below 1.5 kW. In this part of the search we observed a tenfold increase in growth rate, however, practically no change in structure of nanofibers was observed. That is, an increase of growth rate did not result in a gradual change of the angle between the graphene layers and the axis of a nanofiber. This result implies that the relationship between growth rate and internal structure is non-linear. Nevertheless, a drastic change in the internal structure was observed by extending the maximization search in a new reactor designed to work at pressures up to 100 Torr and powers up to 30 kW.

The maximum growth rate in the new reactor was achieved in experiments performed in the range 20–30 Torr (limited by the maximum pressure at which a stable glow discharge could be achieved in this reactor) with 3 A of current. Growth at these pressures resulted in a drastic structure change as shown in Figs. 5(c) and 5(d) and a 100-fold increase in growth rate. At these conditions, the relatively high plasma current increased the temperature of the substrate holder, and thus the actual growth temperature of the sample was estimated to be about 850 °C with an infrared pyrometer. In essence, this high growth rate and structural change was achieved at much higher pressure, temperature, and plasma current than has previously been reported in the literature. Figures 5(c) and 5(d) shows an image of a "fast" growing nanofiber (from maximized conditions) with angle α of about 1° (approaching a multiwall nanotube structure) compared to about 25° for the "slow" growing nanofiber in Figs. 5(a) and 5(b). The fast growth rate (8000 nm/min) exceeded the "slow" growth rate (80 nm/min) by two orders of magnitude. The particle morphology also changed from a teardrop shape to an elongated rectangle as shown in Figs. 5(a) and 5(c). High resolution TEM images in Fig. 6 show the well-ordered graphitic structure of the nearly parallel sidewalls with an average (002) *d* spacing of 3.4 Å. This result confirms the existence of the link between growth conditions, growth rate, and nanofiber internal structure, and suggests that the growth condition can override the structure influence imposed by the preparation of catalyst material.

One of the important implications of this result is that the internal structure can be modulated along the nanofiber by switching growth conditions during the synthesis process. This modulation of structure is demonstrated in Fig. 7, which shows the transition region between fast and slow growth modes. In this example, the fibers were initially grown at a high growth rate to produce nanotubelike fibers with a small cone angle and then conditions were switched to the slow growth regime, producing herringbone structure. In order to switch growth conditions, the plasma was turned off for several seconds while the pressure equilibrated to a new setting. Then the plasma was turned on again and growth resumed, following a brief 10 s pretreatment in ammonia plasma, which removed a thin carbon layer covering the catalyst particle.

The variation of nanoparticle shape in the two growth regimes and the dependence of this shape on crystallographic orientation (as discussed above) have led us to hypothesize that the nanoparticle changes its orientation when transitioning between the two regimes. This seems possible since the shape of the catalyst particle can dynamically change during synthesis, as has been observed by *in situ* TEM.[36] It is also interesting to note that the transition between fast and slow regimes often causes the catalyst nanoparticle to split into two pieces, with one section of catalyst material remaining at the transition point between fast and slow growth. In addition, some nanoparticles exhibited multiple crystalline domains (as seen by diffraction contrast in the TEM, results not shown here), which could be artifacts from the orientational reordering of the particle. However, grazing incidence x-ray diffraction (XRD) shown in Fig. 8 shows no marked differences in the nickel reflections between the slow [Fig. 8(a)] and fast [Fig. 8(b)] growth regimes. In order to avoid a strong Si [311] peak at the grazing angle, the Ni films were deposited onto off-axis wafers (3° off of [100] toward [110]). However, we are still investigating the possibility of highly preferred orientation, which may not manifest observable changes in grazing incidence XRD. Pole figure analysis and

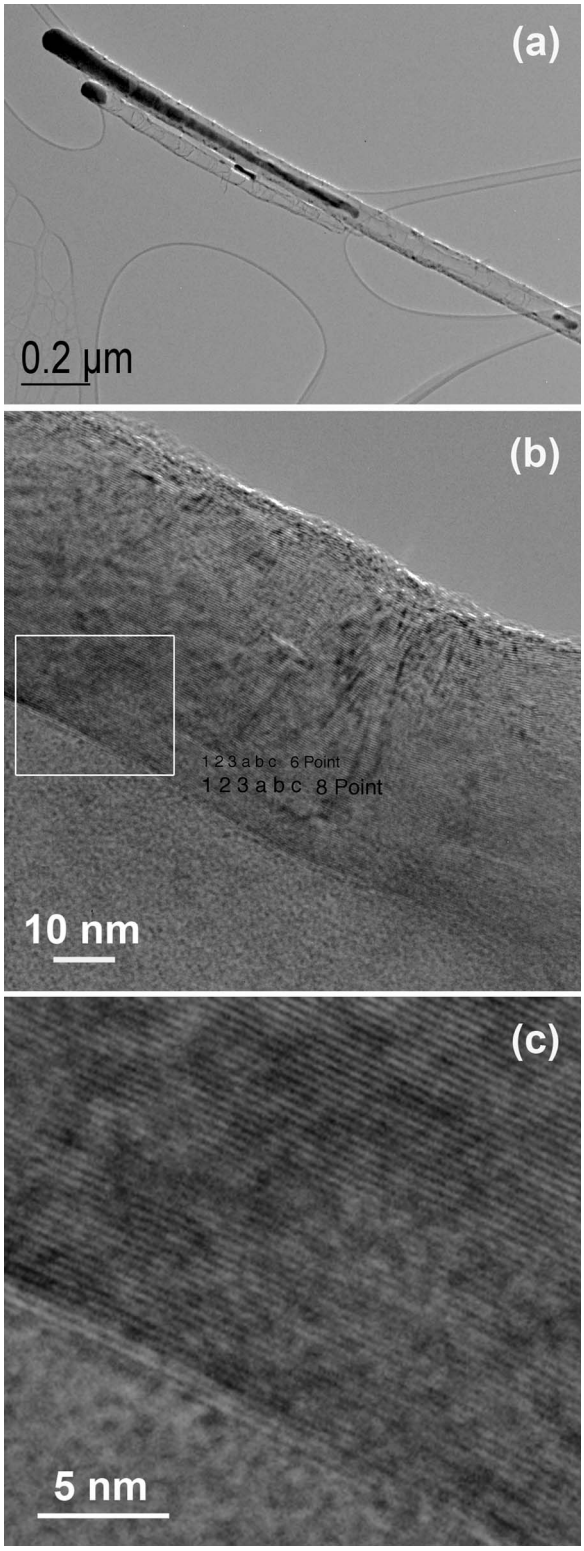

FIG. 6. (a) TEM image of the internal structure of a CNF grown in the fast growth regime with a stretched Ni nanoparticle (dark contrast); (b) high resolution TEM image of the CNF sidewall below the catalyst nanoparticle in (a); (c) magnified view of the area indicated by the rectangle in (b) displaying graphite lattice fringes with average (002) *d* spacing of 3.4 Å.

extensive electron diffraction statistical analysis are necessary to determine if the link between the nanofiber structure changes and the crystallographic orientation of the particles exists.

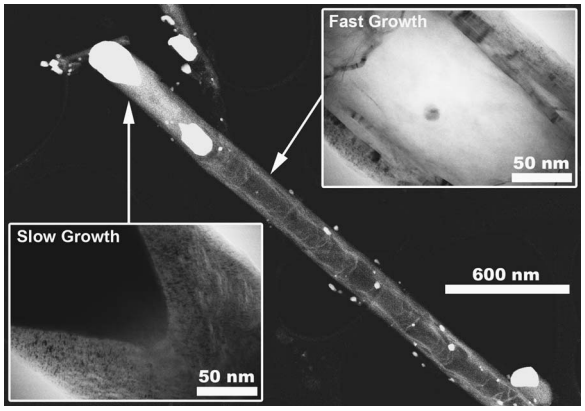

FIG. 7. *z*-contrast STEM image of the modulated structure of a nanofiber grown in a sequence of slow-fast-slow conditions (just the fast-slow portion is shown). The insets show higher magnification transmission images of the slow and fast growth sections.

Modulation of the fiber internal structure has some useful applications. As was discussed earlier, the variation of the internal graphitic structure of the nanofiber inevitably results in a variation of the surface structure. The modulation of the nanofiber structure causes the modulation of graphene edge density along the nanofiber length. Much higher electron transport in the regions featuring high densities of graphene edge planes can be demonstrated by the electrodeposition of metals onto a nanofiber electrode. Figure 9(a) shows gold nanoparticles electrodeposited at the graphene edges of a nanofiber sidewall using a commercially available plating solution (Orotherm Gold HT). This phenomenon should allow favored attachment of gold at the regions that have a higher density of exposed edges, providing a strategy for preferential decoration and subsequent biochemical modification along the nanofiber length. Figure 9(b) shows a variation of electroplated Au nanoparticle density along a nanofiber that was synthesized in a fast-slow growth regime, indicating a higher density of gold nucleation within the edge-plane-rich, slow growth region.

III. CONCLUSIONS

We have demonstrated that the internal structure of VACNFs grown by catalytic PECVD can be influenced by

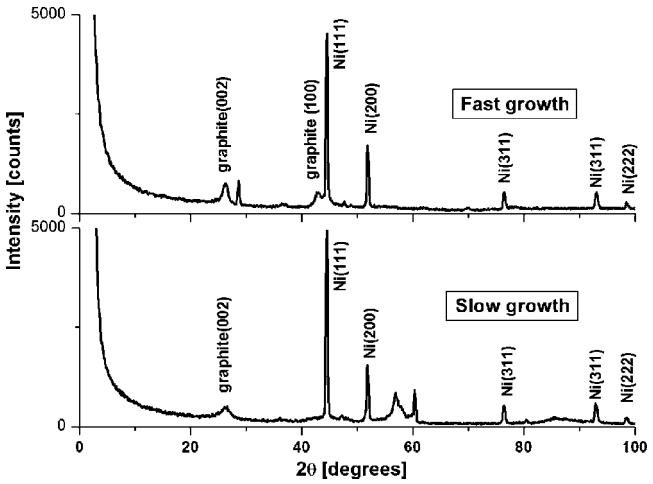

FIG. 8. XRD grazing incidence scans of substrates after fast and slow fiber growth regimes.

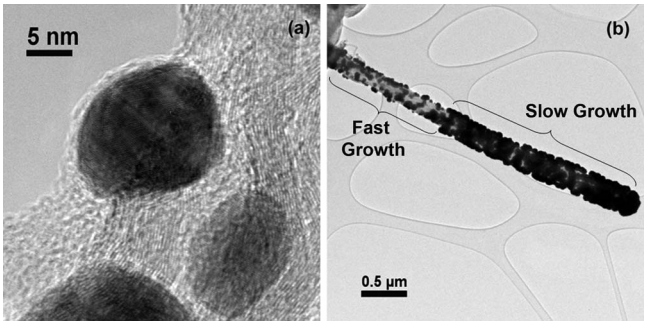

FIG. 9. (a) TEM image of gold nanoparticles nucleated after electroplating on the graphene edges of a nanofiber sidewall; (b) TEM image of a VACNF grown in a modulated regime (fast-slow) with Au nanoparticles electroplated along the nanofiber sidewalls.

the crystallographic orientation, the structure, and the shape of the catalytic nanoparticle. However, growth conditions are an overriding factor in determination of the internal nanofiber structure. The synthesis conditions that correspond to higher growth rate produce nanofibers with only slightly angled graphene layers, approaching the structure of multiwalled carbon nanotubes. The variation of synthesis conditions during nanofiber growth allows for the modulation of internal structure and surface properties along the length of the nanofiber.

ACKNOWLEDGMENTS

M.L.S., A.V.M., I.A.M., and J.A.H. acknowledge support from the Material Sciences and Engineering Division Program of the DOE Office of Science. K.L.K. and P.D.R. acknowledge support from the Center for Nanophase Materials Sciences (CNMS). TEM was supported in part by the National Institute for Biomedical Imaging and Bioengineering Grant No. R01EB006316. A portion of this research was conducted at the Center for Nanophase Materials Sciences, which is sponsored at Oak Ridge National Laboratory by the Division of Scientific User Facilities (DOE).

[1]P. W. Anderson, Science **177**, 393 (1972).
[2]M. S. Dresselhaus, "Carbon: Bonding," in *Encyclopedia of Materials: Science and Technology* (Elsevier Science Ltd., New York, 2001).
[3]H. W. Kroto, J. R. Heath, S. C. Obrien, R. F. Curl, and R. E. Smalley, Nature (London) **318**, 162 (1985).
[4]S. Iijima, Nature (London) **354**, 56 (1991).
[5]M. Terrones and H. Terrones, Philos. Trans. R. Soc. London, Ser. A **361**, 2789 (2003).
[6]A. Krishnan, E. Dujardin, M. M. J. Treacy, J. Hugdahl, S. Lynum, and T. W. Ebbesen, Nature (London) **388**, 451 (1997).
[7]A. Javey, J. Guo, Q. Wang, M. Lundstrom, and H. J. Dai, Nature (London) **424**, 654 (2003).
[8]M. F. Yu, O. Lourie, M. J. Dyer, K. Moloni, T. F. Kelly, and R. S. Ruoff, Science **287**, 637 (2000).
[9]S. E. Baker, K. Y. Tse, C. S. Lee, and R. J. Hamers, Diamond Relat. Mater. **15**, 433 (2006).
[10]S. E. Baker, K. Y. Tse, E. Hindin, B. M. Nichols, T. L. Clare, and R. J. Hamers, Chem. Mater. **17**, 4971 (2005).
[11]B. L. Fletcher, T. E. McKnight, A. V. Melechko, M. L. Simpson, and M. J. Doktycz, Nanotechnology **17**, 2032 (2006).
[12]T. E. McKnight, C. Peeraphatdit, S. W. Jones, J. D. Fowlkes, B. L. Fletcher, K. L. Klein, A. V. Melechko, M. J. Doktycz, and M. L. Simpson, Chem. Mater. **18**, 3203 (2006).
[13]S. E. Baker, P. E. Colavita, K. Y. Tse, and R. J. Hamers, Chem. Mater. **18**, 4415 (2006).
[14]T. E. McKnight, A. V. Melechko, D. W. Austin, T. Sims, M. A. Guillorn, and M. L. Simpson, J. Phys. Chem. B **108**, 7115 (2004).
[15]T. E. McKnight, A. V. Melechko, B. L. Fletcher, S. W. Jones, D. K. Hensley, D. B. Peckys, G. D. Griffin, M. L. Simpson, and M. N. Ericson, J. Phys. Chem. B **110**, 15317 (2006).
[16]M. Endo, Y. A. Kim, T. Hayashi, Y. Fukai, K. Oshida, M. Terrones, T. Yanagisawa, S. Higaki, and M. S. Dresselhaus, Appl. Phys. Lett. **80**, 1267 (2002).
[17]N. M. Rodriguez, A. Chambers, and R. T. K. Baker, Langmuir **11**, 3862 (1995).
[18]R. L. McCreery, in *Electroanalytical Chemistry*, edited by A. J. Bard (Marcel Dekker, New York, 1991), p. 221.
[19]V. I. Merkulov, D. H. Lowndes, Y. Y. Wei, G. Eres, and E. Voelkl, Appl. Phys. Lett. **76**, 3555 (2000).
[20]Z. F. Ren, Z. P. Huang, D. Z. Wang, J. G. Wen, J. W. Xu, J. H. Wang, L. E. Calvet, J. Chen, J. F. Klemic, and M. A. Reed, Appl. Phys. Lett. **75**, 1086 (1999).
[21]M. Chhowalla, K. B. K. Teo, C. Ducati, N. L. Rupesinghe, G. A. J. Amaratunga, A. C. Ferrari, D. Roy, J. Robertson, and W. I. Milne, J. Appl. Phys. **90**, 5308 (2001).
[22]J. Koehne, H. Chen, J. Li, A. M. Cassell, Q. Ye, H. T. Ng, J. Han, and M. Meyyappan, Nanotechnology **14**, 1239 (2003).
[23]X. J. Yang, M. A. Guillorn, D. Austin, A. V. Melechko, H. T. Cui, H. M. Meyer, V. I. Merkulov, J. B. O. Caughman, D. H. Lowndes, and M. L. Simpson, Nano Lett. **3**, 1751 (2003).
[24]J. Moser, R. Panepucci, Z. P. Huang, W. Z. Li, Z. F. Ren, A. Usheva, and M. J. Naughton, J. Vac. Sci. Technol. B **21**, 1004 (2003).
[25]Q. Ye, A. Cassell, H. Liu, K.-J. Chao, J. Han, and M. Meyyappan, Nano Lett. **4**, 1301 (2004).
[26]M. A. Guillorn, X. Yang, A. V. Melechko, D. K. Hensley, M. D. Hale, V. I. Merkulov, M. L. Simpson, L. R. Baylor, W. L. Gardner, and D. H. Lowndes, J. Vac. Sci. Technol. B **22**, 35 (2004).
[27]T. E. McKnight, A. V. Melechko, D. K. Hensley, D. G. J. Mann, G. D. Griffin, and M. L. Simpson, Nano Lett. **4**, 1213 (2004).
[28]J. D. Fowlkes, A. V. Melechko, K. L. Klein, P. D. Rack, D. A. Smith, D. K. Hensley, M. J. Doktycz, and M. L. Simpson, Carbon **44**, 1503 (2006).
[29]N. A. Kiselev, J. L. Hutchison, A. P. Moravsky, E. V. Rakova, E. V. Dreval, C. J. D. Hetherington, D. N. Zakharov, J. Sloan, and R. O. Loutfy, Carbon **42**, 149 (2004).
[30]D. Golberg, C. Z. Gu, Y. Bando, M. Mitome, and C. C. Tang, Acta Mater. **53**, 1583 (2005).
[31]D. Lupu, A. R. Biris, I. Misan, A. Jianu, G. Holzhuter, and E. Burkel, Int. J. Hydrogen Energy **29**, 97 (2004).
[32]S. H. Tsai, C. W. Chao, C. L. Lee, and H. C. Shih, Appl. Phys. Lett. **74**, 3462 (1999).
[33]M. L. Mabudafhasi, R. Bodkin, C. P. Nicolaides, X. Y. Liu, M. J. Witcomb, and N. J. Coville, Carbon **40**, 2737 (2002).
[34]K. L. Klein, A. V. Melechko, P. D. Rack, J. D. Fowlkes, H. M. Meyer, and M. L. Simpson, Carbon **43**, 1857 (2005).
[35]L. Dong, J. Jiao, C. Pan, and D. W. Tuggle, Appl. Phys. A **78**, 9–14 (2004).
[36]S. Helveg, C. Lopez-Cartes, J. Sehested, P. L. Hansen, B. S. Clausen, J. R. Rostrup-Nielsen, F. Abild-Pedersen, and J. K. Norskov, Nature (London) **427**, 426 (2004).
[37]V. I. Merkulov, D. K. Hensley, A. V. Melechko, M. A. Guillorn, D. H. Lowndes, and M. L. Simpson, J. Phys. Chem. B **106**, 10570 (2002).
[38]V. I. Merkulov, A. V. Melechko, M. A. Guillorn, D. H. Lowndes, and M. L. Simpson, Chem. Phys. Lett. **361**, 492 (2002).
[39]A. V. Merkulov, I. A. Meleshko, J. C. Wells, H. Cui, V. I. Merkulov, M. L. Simpson, and D. H. Lowndes, Phys. Rev. B **72**, 045409 (2005).
[40]G. Eres, A. A. Puretzky, D. B. Geohegan, and H. Cui, Appl. Phys. Lett. **84**, 1759 (2004).
[41]V. Merkulov, A. V. Melechko, M. A. Guillorn, D. H. Lowndes, and M. L. Simpson, Chem. Phys. Lett. **361**, 492 (2002).
[42]V. I. Merkulov, M. A. Guillorn, D. H. Lowndes, M. L. Simpson, and E. Voelkl, Appl. Phys. Lett. **79**, 1178 (2001).